

Transverse modulational instability in counterpropagating two-wave mixing with frequency-detuned pump beams

M. Schwab and C. Denz*

Institute of Applied Physics, Darmstadt University Of Technology, Hochschulstrasse 6, D-64289 Darmstadt, Germany

M. Saffman[†]

Department of Optics and Fluid Dynamics, Risø National Laboratory, DK-4000 Roskilde, Denmark

Received July 19, 2000; revised manuscript received November 27, 2000

We report theoretical and experimental evidence for transverse modulational instability of two counterpropagating beams in a photorefractive medium with no external feedback. A frequency detuning is applied to one of the beams in order to drive the system to instability. We perform a linear-stability analysis that allows for detuning of the counterpropagating pump beams in addition to an additional frequency detuning of the generated sidebands relative to the main beams. The threshold condition for the general case of a complex photorefractive coupling constant is found, and instability is predicted for diffusion-dominated, drift-dominated, and mixed charge transport. We show that for the specific case of diffusion-dominated charge transport, transverse instability is always accompanied by a frequency shift of the sidebands. For frequency-degenerate pump beams the instability threshold is reached at a coupling-constant times interaction-length product of $\gamma l = 5.25i$. The threshold is lowered (raised) for small positive (negative) frequency shifts of one of the pump beams. The theoretical predictions were verified experimentally with a photorefractive crystal of KNbO₃. A modulational instability resulting in a spatially periodic roll pattern was observed for a certain range of positive frequency detunings. Measurements of the transverse scale of the structures and the relative sideband intensities were in agreement with the theoretical analysis. © 2001 Optical Society of America

OCIS codes: 190.0190, 190.4420, 190.5330.

1. INTRODUCTION

The spontaneous formation of periodic spatial structures in physical, chemical, or biological systems has attracted considerable interest.^{1,2} When excited beyond a certain instability threshold, all these different systems show self-organized behavior that is described by universal order parameter equations. A common situation is modulational instability of a spatially uniform ground state that leads to the spontaneous formation of spatial patterns. These patterns often have simple geometric structures, e.g., hexagonal patterns are predominant in many cases. Nonlinear optical materials are well suited for the observation of these transverse modulational instabilities. They provide the possibility of pattern observation at moderate laser powers. Control parameters are easily accessible, and the time constants for the systems allow for quantitative measurements in real time. Moreover, possible technological applications of pattern formation in the field of optical information processing³ motivate ongoing intensive research.

Transverse modulational instability of two counterpropagating beams has been observed and investigated theoretically in a large number of nonlinear optical media. Atomic vapors,^{4–6} liquid crystals (Kerr media),^{7–10} liquid-crystal light valves,^{11,12} organic films,¹³ and photorefractives^{14,15} all show similar behavior when excited beyond threshold. The pump beams, either exter-

nally supplied or with a counterpropagating beam created by a feedback mirror, become modulationally unstable, and arrays of spots, most likely with hexagonal symmetry, appear in the optical far field. The angle θ between the pump and the generated satellite beams can be predicted by a linear-stability analysis that also gives information on the threshold of modulational instability.

Owing to the relative slowness of the photorefractive response and the large nonlinearity of these materials even at low laser powers, these phenomena have been thoroughly studied in photorefractive crystals such as potassium niobate (KNbO₃), barium titanate (BaTiO₃), and strontium barium niobate (SBN) in recent years. Because of variations in the structure of the electro-optic tensor in different photorefractive materials, it is necessary to distinguish between two distinct ways of coupling counterpropagating beams. In the case of a transmission-grating interaction the counterpropagating pump beams do not scatter into each other, and there is no direct coupling of energy or phase between the pump beams. Nonetheless, a modulational instability can occur in Kerr⁸ and photorefractive¹⁶ media and has been observed in strontium barium niobate with an externally applied electric field.¹⁷

Alternatively it is possible to use a crystal orientation that results in formation of strong reflection gratings owing to a direct interference of the pump beams and negli-

gible transmission gratings. In this case there is a direct coupling of energy and phase between the pump beams that complicates the theoretical analysis considerably. Two types of reflection-grating-mediated interaction geometry have been considered: externally supplied pump beams with no external feedback and the case in which a single pump beam as well as the generated sidebands are reflected by an external mirror. Although both types of boundary condition were used in the first reported observation of hexagons in KNbO_3 ,¹⁴ all the subsequent experimental studies, including Refs. 15 and 18–21, have used mirror boundary conditions. Besides the difference in the threshold of the instability in these two geometries, the transverse scale of the pattern is different. In the case of external beams the pattern scale is proportional to $\sqrt{\lambda L}$, where λ is the optical wavelength and L is the length of the nonlinear medium. For a thin medium and a long external feedback path to the mirror the pattern scale is proportional to $\sqrt{\lambda L_f}$, where L_f is the distance to the mirror, whereas in the general case in which the thickness of the medium is comparable with the distance to the mirror, the pattern scale depends on both L and L_f . It is worth noting that there is also an intermediate situation in which the generated sidebands, but not the pump beam, are reflected by an external mirror that leads to a unique regime of pattern formation.²²

In parallel with the experimental studies that used mirror boundary conditions, a number of theoretical studies have given an improved insight into the stages of pattern formation in reflection-grating-dominated photorefractive materials.^{19,23–27} These studies have considered many aspects of the reflection-grating interaction, including a linear-stability analysis, taking into account the intensity profile and variation of the total intensity across the crystal for the case of energy coupling between the two counterpropagating beams. A nonlinear analysis for such a system with a feedback mirror was published recently,²⁸ providing the proof that hexagons are predominant for small positive values of the diffraction length L . Also the appearance of other geometric structures such as squares^{18–20} and studies of pattern dynamics owing to angular misalignment^{19,21} were reported in the feedback-mirror arrangement.

It is apparent that photorefractive feedback systems with reflection-grating interactions have been widely discussed; nonetheless, there remain some open questions. One of these is the question of instability with externally supplied pump beams. Although this case was originally investigated by Honda,¹⁴ the interpretation of those experiments is unclear, since the second pump beam was in fact provided by reflection from a phase-conjugate mirror. Furthermore, the calculations of transverse instability for external-beam boundary conditions and energy coupling between the pump beams²³ were marred by an error in calculation. The same mistake was corrected for the case of phase coupling in Ref. 25 but has not yet been remedied for energy coupling that corresponds to the experimental conditions in Ref. 14.

Our focus of interest in this paper is to make a detailed theoretical study of the external-beam reflection-grating geometry. We rectify the earlier analysis of Saffman *et al.*²³ and find the correct value of the coupling strength

at instability. In addition we include the possibility of a frequency shift between the externally supplied pump beams that effectively makes the coupling constant complex. We show the equivalence of this method to that of an externally applied field²⁷ and demonstrate that the frequency shift has important consequences for both the threshold and the resulting spatial scale of the instability. In addition we study the external-beam case experimentally and demonstrate the presence of an instability both with and without frequency shift of the pump beams. Since the original external-pump-beam experiment of Honda¹⁴ with a phase-conjugate mirror to generate the second pump beam may also have resulted in a frequency shift of the pump beams, we provide a discussion of those early experimental results.

The paper is structured as follows: In Section 2 we review the basic model equations for photorefractive two-wave mixing in counterpropagating geometry and perform in detail the linear-stability analysis for the configuration with two external frequency-detuned beams. Extending previous analysis,²⁴ we take into account a possible frequency detuning of the emitted sidebands and derive, for the sake of generality, a threshold equation for complex values of the photorefractive coupling constant γ . Important conclusions are drawn for the experimentally relevant choice of an imaginary coupling constant. In order to verify the theoretical analysis we performed an experiment with a photorefractive KNbO_3 crystal and two external beams that entered the crystal from opposite directions, where one of the beams was slightly detuned in frequency by means of a piezo-driven mirror. The details of the experiment are described in Section 3. Section 4 is devoted to detailed discussions and additional calculations. A comparison with the theoretical analysis completes this part. Section 5 summarizes the main results and accentuates the conclusions of this paper.

2. LINEAR-STABILITY ANALYSIS

The basic interaction geometry under consideration is depicted in Fig. 1. Let us consider two plane waves $F(z) = F_0 \exp[i(k_0 z - \omega_0 t)]$ and $B(z) = B_0 \exp[-i(k_0 z + \omega_0 t + \Omega t)]$ entering a photorefractive crystal from opposite sides, where ω_0 denotes the optical frequency of the laser light, and k_0 is the corresponding wave vector. We account for a possible frequency detuning Ω of the two counterpropagating beams. In this configuration a reflection grating is formed that redistributes energy and/or phase between the two counterpropagating beams. The grating

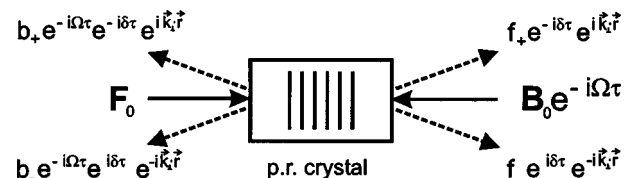


Fig. 1. Basic interaction geometry. Two externally supplied counterpropagating beams with a relative frequency detuning Ω write a reflection grating inside the crystal. The created sidebands with an additional frequency shift δ and transverse \mathbf{k} vector \mathbf{k}_\perp are also indicated.

vector $k_g = 2k_0$ is collinear with the propagation directions of both beams. We also allow for a possible frequency detuning δ of the sidebands relative to the carrier. All interactions between the sidebands themselves will be assumed to be sufficiently small and are thus neglected.^{19,23,24}

The equations of motion we start from are the photorefractive two-wave mixing equations including diffraction. These equations and the relaxation equation for the grating amplitude can be written in the paraxial approximation as^{24,27}

$$\frac{\partial F}{\partial z} - \frac{i}{2k_0 n_0} \nabla_{\perp}^2 F = gB, \quad (1)$$

$$\frac{\partial B}{\partial z} + \frac{i}{2k_0 n_0} \nabla_{\perp}^2 B = g^*F, \quad (2)$$

$$\left(\tau \frac{\partial}{\partial t} + 1 \right) g = i\gamma \frac{FB^*}{|F|^2 + |B|^2}. \quad (3)$$

Equations (1) and (2) stem from the usual coupled-wave theory, taking into account the photorefractive material response found by Kukhtarev *et al.*²⁹ z is the direction of propagation as indicated in Fig. 1, n_0 denotes the (linear) refractive index of the material, x and y are transverse coordinates and ∇_{\perp}^2 represents the transverse Laplacian $\nabla_{\perp}^2 = \partial^2/\partial x^2 + \partial^2/\partial y^2$, g is the amplitude of the photorefractive index grating, and $\gamma = \pi n_1/\lambda \exp(-i\phi)$ is the complex photorefractive coupling constant, which is a measure for amplitude and phase transfer in the photorefractive mixing process.³⁰ Here, λ is the vacuum wavelength of the incident waves and n_1 represents a dimensionless measure for the modulation depth of the index grating. ϕ is the relative phase shift between the light-intensity pattern formed by the two counterpropagating beams and the resulting photorefractive index pattern. For drift-dominated material such as LiNbO₃, this phase shift is nearly zero, leading to a purely real coupling constant.³⁰ Diffusion-dominated materials such as KNbO₃ or BaTiO₃ show phase shifts of close to $\phi = \pi/2$, yielding a purely imaginary coupling constant. In the latter case this phase shift is responsible for beam coupling (energy transfer) between the two counterpropagating beams. Equation (3) describes the dynamics of the photorefractive grating with grating amplitude g , τ being the relaxation constant for the photorefractive index grating. Note that Eq. (3) is strictly accurate only for weak modulation of the interference pattern created by F and B . The effect on the transverse instability of corrections that account for the dependence of the coupling constant γ on the modulation depth has been investigated in Ref. 27.

The two counterpropagating beams F and B may be unstable against perturbations in the transverse plane. An appropriate perturbation ansatz for the plane-wave solutions is

$$F(z) = \bar{F}_0(z) \{ 1 + f_+ \exp[i(\mathbf{k}_{\perp} \cdot \mathbf{r} - \delta t)] + f_- \exp[-i(\mathbf{k}_{\perp} \cdot \mathbf{r} - \delta t)] \}, \quad (4)$$

$$B(z) = \bar{B}_0(z) \{ 1 + b_+ \exp[i(\mathbf{k}_{\perp} \cdot \mathbf{r} - \delta t)] + b_- \exp[-i(\mathbf{k}_{\perp} \cdot \mathbf{r} - \delta t)] \}, \quad (5)$$

with

$$\bar{F}_0(z) = F_0(z) \exp[i(k_0 z - \omega_0 t)], \quad (6)$$

$$\bar{B}_0(z) = B_0(z) \exp[i(-k_0 z - \omega_0 t)] \exp(-i\Omega t), \quad (7)$$

where f_+ , f_- , b_+ , and b_- are the relative amplitudes of the weak sidebands. Two important ingredients will be taken into account that generalize earlier studies: a frequency detuning between the two pump beams Ω is assumed; additionally we allow for a possible frequency detuning δ of the sidebands relative to the pump in Eqs. (4) and (5) that leads to a transverse traveling wave. We insert the perturbation ansatz (4) and (5) into the equation for the material response (3) and expand the denominator of the right-hand side of Eq. (3) in a manner similar to the derivation given in Ref. 24. This leads to the following equation for the grating amplitude g :

$$\begin{aligned} \left(\tau \frac{\partial}{\partial t} + 1 \right) g = & r_0 \exp(i\Omega t) + r_0 r_- \\ & \times \exp[i(\mathbf{k}_{\perp} \cdot \mathbf{r} + (\Omega - \delta)t)] \\ & + r_0 r_+ \exp\{i[-\mathbf{k}_{\perp} \cdot \mathbf{r} + (\Omega + \delta)t]\}, \end{aligned} \quad (8)$$

with the terms

$$r_0 = i\gamma \frac{F_0 B_0^*}{|F_0|^2 + |B_0|^2}, \quad (9)$$

$$r_- = \frac{1}{|F_0|^2 + |B_0|^2} [|F_0|^2 (b_-^* - f_-^*) + |B_0|^2 (f_+ - b_+)], \quad (10)$$

$$r_+ = \frac{1}{|F_0|^2 + |B_0|^2} [|F_0|^2 (b_+^* - f_+^*) + |B_0|^2 (f_- - b_-)]. \quad (11)$$

The form of Eq. (8) motivates the following ansatz for the solution of Eq. (3):

$$g(t) = g_0 \exp(i\Omega t) + g_1 \exp\{i[\mathbf{k}_{\perp} \cdot \mathbf{r} + (\Omega - \delta)t]\} + g_2 \exp\{i[-\mathbf{k}_{\perp} \cdot \mathbf{r} + (\Omega + \delta)t]\}. \quad (12)$$

Inserting this equation into Eq. (3) and comparing the coefficients leads to

$$g = \chi_0 r_0 + \chi_- r_0 r_- \exp\{i[\mathbf{k}_{\perp} \cdot \mathbf{r} + (\Omega - \delta)t]\} + \chi_+ r_0 r_+ \exp\{i[-\mathbf{k}_{\perp} \cdot \mathbf{r} + (\Omega + \delta)t]\}, \quad (13)$$

with the abbreviations

$$\chi_0 = \frac{1}{1 + i\Omega\tau}, \quad (14)$$

$$\chi_{\pm} = \frac{1}{1 + i(\Omega \pm \delta)\tau}. \quad (15)$$

Inserting the expression for the grating amplitude of the index grating Eq. (13) into the two-wave mixing equations (1) and (2) leads to the following four equations for the perturbation amplitudes:

$$\begin{aligned}
\left(\frac{\partial}{\partial z} + ik_d\right)f_+ &= -i\gamma A\{\chi_-(f_-^* - b_-^*) \\
&\quad + [\chi_0 + q(\chi_0 - \chi_-)](f_+ - b_+)\}, \\
\left(\frac{\partial}{\partial z} - ik_d\right)f_-^* &= i\gamma^* A\{\chi_+^*(f_+ - b_+) \\
&\quad + [\chi_0^* + q(\chi_0^* - \chi_+^*)](f_-^* - b_-^*)\}, \\
\left(\frac{\partial}{\partial z} + ik_d\right)b_+ &= -i\gamma^* A\{\chi_+^*(f_-^* - b_-^*) \\
&\quad + [\chi_0^* + q^{-1}(\chi_0^* - \chi_+^*)](f_+ - b_+)\}, \\
\left(\frac{\partial}{\partial z} - ik_d\right)b_-^* &= i\gamma A\{\chi_-(f_+ - b_+) \\
&\quad + [\chi_0 + q^{-1}(\chi_0 - \chi_-)](f_-^* - b_-^*)\},
\end{aligned} \tag{16}$$

where A represents the strength of transverse coupling,

$$A = \frac{|F_0|^2|B_0|^2}{(|F_0|^2 + |B_0|^2)^2}, \tag{17}$$

and is connected to the modulation depth of the interference grating, m , by $A = 1/4m^2$. k_d is the characteristic diffraction wave number

$$k_d = \frac{k_\perp^2}{2k_0 n_0}, \tag{18}$$

and q is the intensity ratio of the two interacting beams,

$$q = \frac{|B_0|^2}{|F_0|^2}. \tag{19}$$

The difficulty in solving the set (16) is the z dependence of A and q . Fortunately, for the case $m = 1$ this z dependence vanishes.²⁴ Therefore we set $q = |B_0|^2/|F_0|^2 = 1$, and as a consequence, $A = 1/4$. The set of equations (16) thus reads as

$$\begin{aligned}
\left(\frac{\partial}{\partial z} + ik_d\right)f_+ &= -i\gamma/4[\chi_-(f_-^* - b_-^*) \\
&\quad + (2\chi_0 - \chi_-)(f_+ - b_+)], \\
\left(\frac{\partial}{\partial z} - ik_d\right)f_-^* &= i\gamma^*/4[\chi_+^*(f_+ - b_+) \\
&\quad + (2\chi_0^* - \chi_+^*)(f_-^* - b_-^*)], \\
\left(\frac{\partial}{\partial z} - ik_d\right)b_+ &= -i\gamma^*/4[\chi_+^*(f_-^* - b_-^*) \\
&\quad + (2\chi_0^* - \chi_+^*)(f_+ - b_+)], \\
\left(\frac{\partial}{\partial z} + ik_d\right)b_-^* &= i\gamma/4[\chi_-(f_+ - b_+) \\
&\quad + (2\chi_0 - \chi_-)(f_-^* - b_-^*)].
\end{aligned} \tag{20}$$

For the special case $\Omega = 0$ and $\delta = 0$ these equations can

be shown to be equivalent to the ones given in Ref. 24. Equations (20) can be written in vector form with

$$\mathbf{u} = \begin{bmatrix} f_+ \\ f_-^* \\ b_+ \\ b_-^* \end{bmatrix} \tag{21}$$

as

$$\frac{d}{dz}\mathbf{u} = \mathcal{D}(\gamma, \delta, \Omega, k_d) \cdot \mathbf{u}. \tag{22}$$

This set of coupled ordinary differential equations can be solved with a base transformation method or Laplace transformation as described in Ref. 24. The boundary conditions for the case of external beams can be written as

$$f_+(0) = f_-^*(0) = 0, \tag{23}$$

$$b_+(l) = b_-^*(l) = 0. \tag{24}$$

The resulting equations can be transformed into an equation of the form

$$\mathcal{B} \cdot \begin{bmatrix} b_+(0) \\ b_-^*(0) \end{bmatrix} = 0, \tag{25}$$

and the threshold condition for modulational instability can then be found from $\det \mathcal{B} = 0$. Defining the new variables

$$\begin{aligned}
\rho(\gamma_I, \gamma_R, \Omega, \delta) &= 2\gamma_R[(\chi_0 + \chi_0^*) - (\chi_- + \chi_+^*)] \\
&\quad + 2i\gamma_I[(\chi_0 - \chi_0^*) - (\chi_- - \chi_+^*)],
\end{aligned} \tag{26}$$

$$\begin{aligned}
\zeta(\gamma_I, \gamma_R, \Omega, \delta) &= 2i\gamma_R[(\chi_0 - \chi_0^*) - (\chi_- - \chi_+^*)] \\
&\quad - 2\gamma_I[(\chi_0 + \chi_0^*) - (\chi_- + \chi_+^*)],
\end{aligned} \tag{27}$$

with $\gamma = \gamma_R + i\gamma_I$, the final threshold condition reads

$$\begin{aligned}
\cosh\left(\frac{1}{2}\chi_0\gamma_I l + \frac{1}{8}\zeta l\right) \\
+ \cos(w_1 l)\cos(w_2 l) + \frac{\eta \sin(w_1 l)\sin(w_2 l)}{w_1 w_2} = 0,
\end{aligned} \tag{28}$$

with

$$w_1 = \sqrt{k_d^2 + k_d\chi_0\gamma_R - \frac{1}{4}\chi_0^2\gamma_I^2}, \tag{29}$$

$$w_2 = \sqrt{k_d^2 + \frac{1}{4}k_d\rho - \frac{1}{64}\zeta^2}, \tag{30}$$

$$\eta = -\frac{1}{8}\chi_0\gamma_I\zeta + k_d^2 + (\chi_0\gamma_R + k_d)\left(k_d + \frac{1}{4}\rho\right). \tag{31}$$

Threshold equation (28) can be shown (apart from differences in notation) to be consistent with the expression given in Ref. 25 for the special case $\Omega = 0$ and $\delta = 0$ and

for pure drift-dominated materials (local photorefractive response), $\gamma_I = 0$. The complete equivalence to the case of an applied electric field can be shown by comparing Eq. (28) with Eq. (14) of Ref. 27. Applying an electric field to a crystal gives the same physical picture (i.e., the same threshold condition) as applying a small frequency offset to one of the beams. The threshold equations are therefore identical in mathematical form for these two cases. The functions ρ and ζ can be attributed to the physical quantities $h(\lambda)$ and $g(\lambda)$ in Ref. 27, the only difference being the functional dependence on the frequency detuning and the externally applied electric field, respectively. This correspondence is also clear in the way the coupling constant γ changes. For the case of frequency shift, γ changes according to $\gamma_{\text{freq.-shift}} = \gamma_0 / (1 + i\Omega\tau)$, with γ_0 being the coupling constant with frequency-degenerate beams or no externally applied voltage. On the other hand, for the case of an externally applied field, one can directly conclude from Eqs. (3) and (4) in Ref. 27 the corresponding equation

$$\begin{aligned} \gamma_{\text{ext.appl.field}} &= \gamma_0 \frac{1 + iE_0}{1 + iE_0/(E_d + E_q)} \\ &= \gamma_0 \frac{1 + f_1(E_0, E_d, E_q)}{1 + f_2(E_0, E_d, E_q)}, \end{aligned}$$

where E_0 denotes the externally applied electric field, and E_d and E_q are the characteristic internal fields.²⁹ Though the functional dependence in both cases is different, one can directly see that both methods are capable of breaking the frequency degeneracy by manipulation of the photorefractive coupling constant. For example, a purely imaginary coupling constant (as is the case for KNbO₃) will turn to a complex one with both imaginary and (depending on the size of the detuning or the applied electric field) real contributions.

Note that Eq. (28) represents a complex threshold equation for five variables, k_d , γ_I , γ_R , Ω , and δ . We will now concentrate on the case of a purely imaginary coupling constant that corresponds to the experimental situation in which diffusion-dominated KNbO₃ was used. A typical threshold curve for $\Omega\tau = 1$ is depicted in Fig. 2(a) together with the corresponding values of $\delta\tau$ as shown in Fig. 2(b). The global minimum in Fig. 2(a) indicates the transverse wave number with the largest growth rate when the system is driven beyond the instability threshold. This occurs in the figure for $k_d l \sim 2.5$, which is slightly less than the nominal value of $k_d l = \pi$, which occurs for the generic case of a transmission-grating interaction in a Kerr⁸ or photorefractive medium with unshifted grating.¹⁶ The frequency shift of the spatial sidebands corresponding to this pair of values (γl , $k_d l$) can then be found from Fig. 2(b). There also exists a similar threshold curve that corresponds to positive values of $\delta\tau$ but with larger values for the threshold coupling strength and is therefore not displayed in the figure for clarity. Calculating the minima for each value of the frequency shift of the external beams, $\Omega\tau$, leads to Fig. 3, where the solid curve displays the minimum coupling strength necessary for modulational instability and negative $\delta\tau$ (which we call δ_- instability), and the dashed

curve shows the same for positive values of $\delta\tau$ (which we call δ_+ instability). Besides a small region $0 \leq \Omega\tau \leq 0.075$, the curve corresponding to negative $\delta\tau$ is the lower one. It is clearly apparent that there exists a minimum threshold, $\gamma l = 4.27i$, for pattern formation in this geometry. One can also directly conclude from Fig. 3 that the instability threshold for positive frequency detunings $\Omega\tau$ is smaller than for negative frequency detunings. Thus observation of pattern formation is expected to be more easily achievable for positive frequency detuning than for negative. A coupling strength of $\gamma l = 4.4i$ (as indicated in Fig. 3 as a horizontal line) would then result in an instability for a certain range of positive frequency detunings $\Omega\tau$. On the other hand, for negative frequency detunings this value is not sufficient to observe a modulational instability.

In Fig. 4 the values for the normalized wave number $k_d l$ that are assigned to the threshold coupling strength are shown, also for both signs of $\delta\tau$. Both curves intersect at $\Omega\tau = 0$ but show completely different dependences. Figure 5 displays the corresponding values for

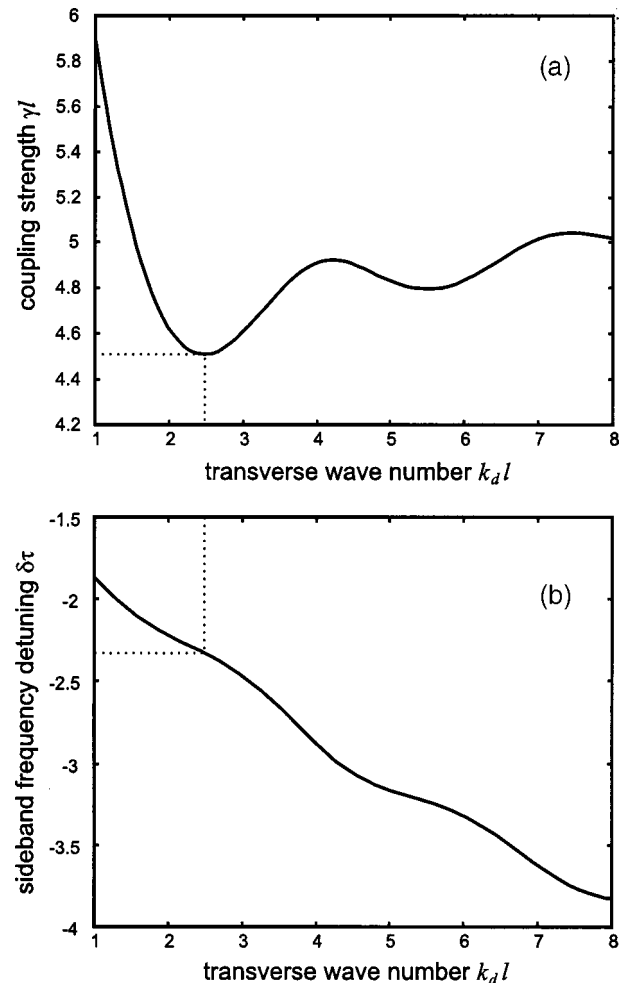


Fig. 2. Threshold curves obtained with Eq. (28) for a parameter value of $\Omega\tau = 1$ and pure energy coupling ($\gamma_R = 0$): (a) Coupling strength γl (normalized coupling constant) as a function of the normalized transverse wave number $k_d l$; (b) corresponding minimum threshold curve for the frequency detuning of the sidebands $\delta\tau$ (normalized to the relaxation constant τ) as a function of the normalized transverse wave number $k_d l$.

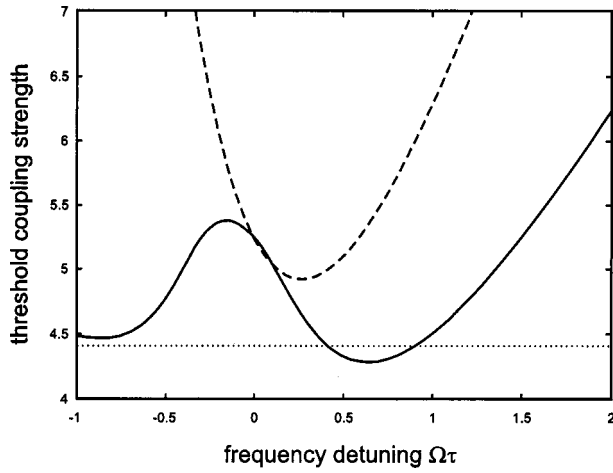


Fig. 3. Threshold coupling strength as a function of the frequency detuning $\Omega\tau$ for pure energy coupling ($\gamma_R = 0$). The minimum values of the coupling strength in the curves similar to Fig. 2 are shown. Solid curve, δ_- instability; dashed curve, δ_+ instability; horizontal line, assumed coupling strength of $\gamma l \approx i4.4$.

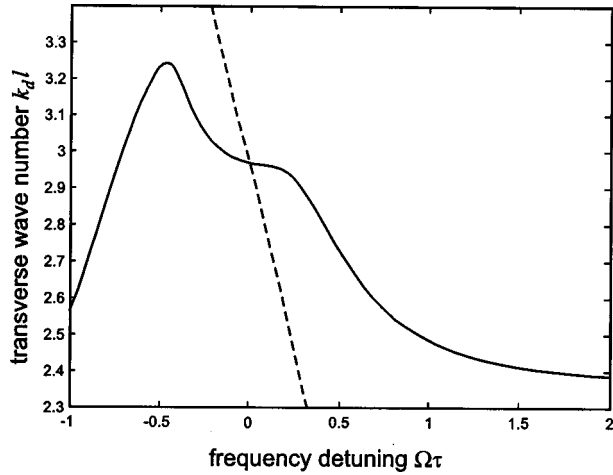


Fig. 4. Transverse pattern scale $k_d l$ as a function of the frequency detuning $\Omega\tau$ corresponding to the coupling strength in Fig. 3. Solid curve, δ_- instability; dashed curve, δ_+ instability.

the frequency shift $\delta\tau$. One can conclude that a frequency shift $\delta\tau$ between the carrier and the sidebands is always present in this geometry.

Let us now focus on the special case of frequency-degenerate pump beams, $\Omega\tau = 0$. In this case, Eq. (28) reduces to

$$\cosh\left[\frac{1}{2}\gamma_I l(1 + \Delta)\right] + \cos(w_{10}l)\cos(w_{20}l) + \frac{\eta_0}{2} \frac{\sin(w_0l)\sin(w_{20}l)}{w_{10}w_{20}} = 0, \quad (32)$$

with the definitions

$$w_{10} = \sqrt{k_d^2 + k_d\gamma_R - \frac{1}{4}\gamma_I^2}, \quad (33)$$

$$w_{20} = \sqrt{k_d^2 - k_d\gamma_R\Delta - \frac{1}{4}\gamma_I^2\Delta^2}, \quad (34)$$

$$\eta_0 = 2k_d^2 + \gamma_R k_d - (\gamma_I^2/2 + \gamma_R^2 + k_d\gamma_R)\Delta, \quad (35)$$

and the abbreviation

$$\Delta = \frac{i\delta\tau}{1 - i\delta\tau}. \quad (36)$$

An important aspect of our analysis is that even for the case $\Omega\tau = 0$ there exists a finite threshold, $\gamma l = 5.25i$, for which pattern formation can be expected with a frequency shift $\delta\tau = \pm 0.97$ and a critical wave number of $k_d l = 2.94$. This corrects the results of Ref. 23, which predicted no instability for this case owing to an incorrect expansion of the denominator in Eq. (3) (see Ref. 24). Since the threshold for modulational δ_+ and δ_- instability is the same for $\Omega\tau = 0$, one can expect both instabilities to occur with the same probability, i.e., spatial sidebands with a certain frequency detuning are induced when the value of the coupling strength exceeds the threshold value of $\gamma l = 5.25i$ given by the linear-stability analysis. This possibility of instability without frequency shift (or without applied electric field) was not discussed in earlier papers^{26,27} and reveals an important aspect of transverse instability in counterpropagating two-wave mixing.

Figure 6 shows the threshold curves for the case of frequency-degenerate beams, $\Omega = 0$, and various values of the coupling constant. In Fig. 6(a) we see that the threshold is raised for $\gamma_R > 0$ and lowered for $\gamma_R < 0$. In Figs. 6(b) and 6(c) we give threshold curves as a function of the real part of the coupling strength, which is relevant for materials with a drift-dominated charge transport. It is noteworthy here that an instability for a purely real coupling strength ($\gamma_I = 0$) occurs without a frequency shift in the sidebands, $\delta = 0$. Figure 6(b) with $\gamma_R < 0$ corresponds to a self-focusing nonlinearity and has a minimum threshold at a finite wave number. Figure 6(c) with $\gamma_R > 0$ corresponds to a self-defocusing nonlinearity, which is known to have a minimum threshold at large wave numbers.⁸ It should be added that a symmetry in γ_I persists for any values of γ_R in the case of de-

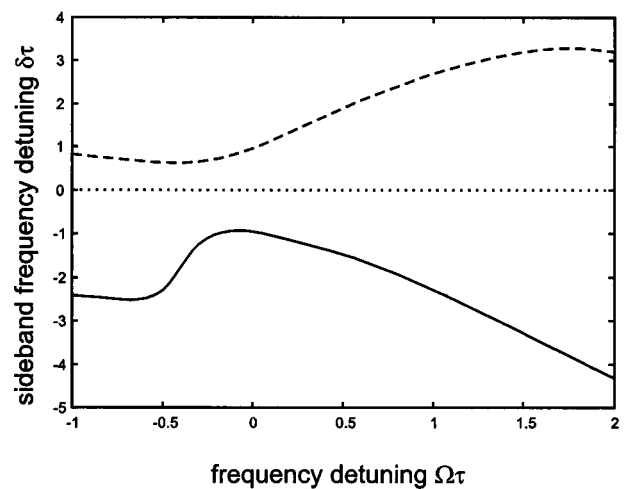


Fig. 5. Frequency detuning of the sidebands with respect to the carrier as a function of the frequency detuning $\Omega\tau$ of the carriers corresponding to Figs. 3 and 4. Solid curve, δ_- instability; dashed curve, δ_+ instability.

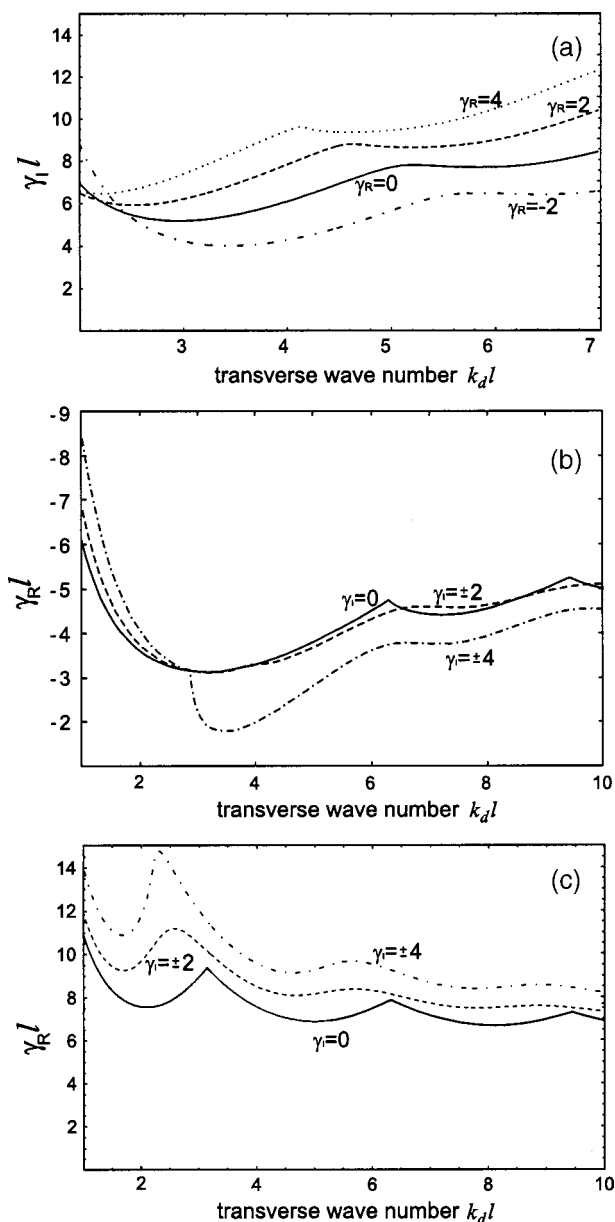


Fig. 6. Threshold curves for $\Omega = 0$: (a) as a function of the imaginary part of the coupling strength and various values of γ_R ; (b), (c) as a function of the real part of the coupling strength and various values of γ_I .

generate pump beams, which can directly be shown with Eqs. (32)–(36) and replacement of γ_I by $-\gamma_I$.

3. EXPERIMENT

The experimental setup is depicted in Fig. 7. The light derived from a frequency-doubled cw Nd:YAG laser operating at a wavelength of 532 nm passes an optical diode and a variable attenuator before it is focused into the photorefractive crystal by a lens with a focal length of $f = 600$ mm. A wedge splits the beam into two parts that are incident from opposite sides on the crystal. The crystal is a heavily iron-doped piece of KNbO₃ with a length of $l = 5$ mm along the crystallographic c axis and a large absorption of up to $\alpha l = 1.2$ depending on the incident intensities. The position of the KNbO₃ crystal is chosen in such a way that the beam waists of both beams overlap inside the crystal. We inclined the crystal by approximately 4° to avoid undesired backreflections from the surface of the crystal producing a perturbation of the pattern-forming process. The beam diameter inside the crystal was measured to be $320 \mu\text{m}$. The reflection-grating interaction in KNbO₃ is known to cause energy coupling between the two counterpropagating beams. The direction of amplification (i.e., the direction of the c axis of the crystal) was chosen so that the amplified part of the beam in the direction of B could be used for examination. Another variable attenuator is used for controlled adjustment of the relative intensities of both beams. One of the beams is reflected at a piezo-controlled mirror providing the frequency detuning between both beams. Our special aim is to perform the measurement for exact counterpropagation and to exclude any sources of feedback. In order to minimize the misalignment by the moving piezo mirror, the angle of incidence is chosen to be as close as possible to a perpendicular incidence ($\epsilon \approx 2^\circ$ to the mirror normal). We used an electronically controlled piezo driver with a large expansion of $30 \mu\text{m}$ to ensure optimum stability of the frequency shift. A voltage ramp applied to the piezo driver thus results in a constant frequency shift of the reflected beam, with a linear dependence on the slope of the ramp: $\Omega = (4\pi/\lambda)v_{\text{Piezo}} \cos \epsilon$, where ϵ is the (small) angle between the incident beam and the mirror normal. Beam splitter BS1 is used to couple out a part of the beam for

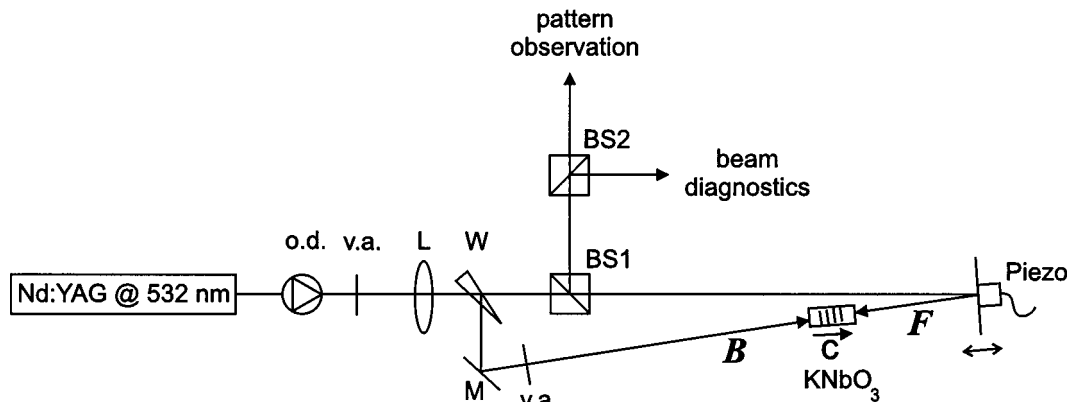


Fig. 7. Experimental setup: o.d., optical diode; v.a.'s, variable attenuators; L, lens; W, wedge; M, mirror; Piezo, piezo-controlled mirror; BS's, beam splitters. The c axis of the crystal indicates the direction of energy transfer.

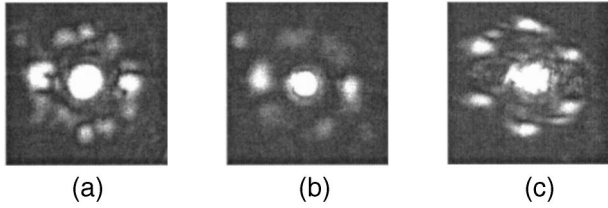


Fig. 8. Experimentally found transverse instabilities: (a) $\Omega = 18$ Hz, roll pattern and underlying instabilities; (b) $\Omega = 34$ Hz, roll pattern with weak coexisting hexagon; (c) nonstationary hexagon for $\Omega = 0$ and slight externally applied misalignment of 0.1° .

pattern observation and recording, and, by beam splitter BS2, for beam diagnostics (e.g., measurement of relative sideband intensities). In order to ensure a constant beam-intensity ratio inside the crystal, which is assumed in the theoretical analysis, we have to account for the energy exchange between the two beams. The depletion of the incoming beam I_1 in the negative direction of the c axis can be determined by³⁰

$$d = |F_0(L)|^2/|F_0(0)|^2 = (1 + M)/[M + \exp(\gamma l)], \quad (37)$$

with M defined as the external beam ratio $M = |F_0(0)|^2/|B_0(L)|^2$. The beam ratio $q(z) = |B_0(z)|^2/|F_0(z)|^2$ therefore is unity at $z = L$ for $M = 1/d$. However, in an experiment we have to choose a value of M slightly smaller than $1/d$ to compensate for the absorption in the crystal such that the average beam ratio becomes unity. The power incident on the crystal was $P_1 = 36$ mW for beam F and $P_2 = 3.6$ mW for beam B , which leads to an external intensity ratio of $M = P_1/P_2 = 10$. The measured depletion was $d = 0.07$, which leads to a coupling strength of $\gamma l \approx 5$. We have to mention here that large modulation-depth effects and absorption are not accounted for, and therefore the above result can only be regarded as a rough estimate. The measured absorption coefficient was $\alpha l = 1.2$ for the same intensities as above.

As predicted by the linear-stability analysis presented in Section 2, we found experimentally a modulational instability for the case of exactly counterpropagating, but frequency-shifted, external beams for a frequency interval $2 \text{ Hz} \leq \Omega \leq 40 \text{ Hz}$. In Figs. 8(a) and 8(b), examples for the resulting transverse structures in the far field for a frequency detuning of $\Omega = 18$ Hz and $\Omega = 34$ Hz are shown. The structures were stationary in space but nonstationary in time with the beat frequency Ω . It is noteworthy that, in this case, a roll pattern was the predominant solution that the system selects. In Fig. 8(a) a roll pattern is predominant, but also other instabilities on the instability circle are visible, but underlying. For larger frequency detunings Ω the amplitudes of these underlying solutions decrease [Fig. 8(b)], and a roll pattern with a weak underlying hexagonal pattern persists up to a border of ~ 40 Hz. Without any frequency shift, $\Omega \tau = 0$, and perfectly counterpropagating beams, no instability can be found, though predicted by our previous analysis. This can be attributed to a coupling constant that is sufficient for pattern formation for nonzero Ω but not for $\Omega = 0$; thus $|\gamma l| < 5.25$. However, in this case an instability

can be induced by a deliberate slight misalignment (of the order of $\sim 0.1^\circ$, which is $\sim 15\%$ of the angle of the sidebands) of the beams relative to each other. Figure 8(c) shows that in this case a full nonstatic hexagonal structure develops.³¹ The misalignment can be regarded as an artificial creation of a frequency detuning. It can be shown that a broken Bragg condition leads to an effective change in phase of the coupling constant in a fashion that is similar to the effect of a frequency detuning.³² Thus both Bragg mismatch and frequency shift can enhance four-wave-mixing interactions.^{32,33} It should be noted that for negative values of Ω , no modulational instability could be found with exactly counterpropagating beams. This is consistent with the linear-stability analysis presented in Section 2 (see Fig. 3), which shows a clear asymmetry in Ω .

4. DISCUSSION

In order to compare the theoretical and experimental investigations we performed measurements of the relative sideband intensity and the transverse wave number of the resulting pattern as a function of the frequency detuning Ω . We found a clear dependence of the relative sideband intensity I_S (integrated intensity over the instability circle divided by the pump intensity) on the frequency detuning with a maximum at $\Omega \approx 20$ Hz. On the other hand, the curve displayed in Fig. 3 shows a minimum of the threshold coupling strength for a certain value of $\Omega \tau$. To determine the unknown relaxation parameter τ , we use a phenomenological model to describe the relative sideband intensity. The buildup of the relative intensity in the sidebands I_S can be described by a simple growth model,³⁴

$$\tau \frac{dI_S}{dt} = \frac{2(\gamma - \gamma_{\text{th}})}{\gamma_{\text{th}}} I_S. \quad (38)$$

Here, γ_{th} denotes the theoretical threshold value for the coupling constant as used in Section 3. This equation has the solution

$$I_S(t) = I_S(0) \exp\left(2 \frac{\gamma - \gamma_{\text{th}}}{\gamma_{\text{th}}} \frac{t}{\tau}\right). \quad (39)$$

Without saturation the sideband intensity goes to infinity. So we add phenomenologically the first saturating term, which should be quadratic in intensity, and get

$$\tau \frac{dI_S}{dt} = \frac{2(\gamma - \gamma_{\text{th}})}{\gamma_{\text{th}}} I_S - \beta I_S^2, \quad (40)$$

where β represents a measure for the strength of the nonlinear saturation process. The steady-state value condition, $dI_S/dt = 0$, thus leads to an equation for the sideband intensity in steady state, \bar{I}_S :

$$\bar{I}_S = \frac{2}{\beta} + \frac{2\gamma}{\beta\gamma_{\text{th}}}. \quad (41)$$

We now take the experimental values for the steady-state sideband intensity and the theoretical values for $\gamma_{\text{th}} = \gamma_{\text{th}}(\Omega \tau)$ and use a least-square-fit method to fit the unknowns β and γ to determine the optimum time con-

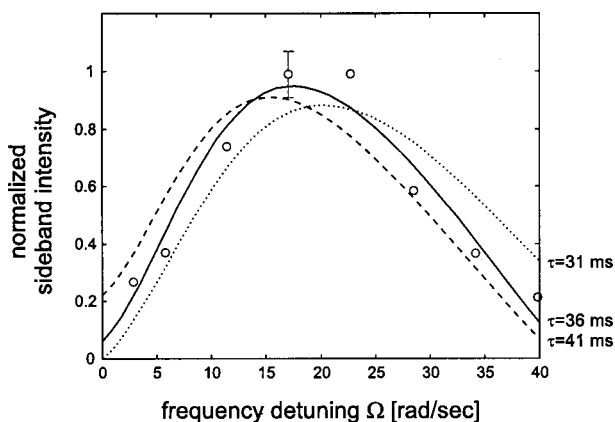


Fig. 9. Relative sideband intensity (integrated sideband intensity with respect to the central beam) versus frequency detuning Ω for $\tau = 36$ ms (solid curve), $\tau = 31$ ms (dotted curve), and $\tau = 41$ ms (dashed curve) as predicted by the linear-stability analysis. Circles represent experimental values normalized to the maximum sideband intensity.

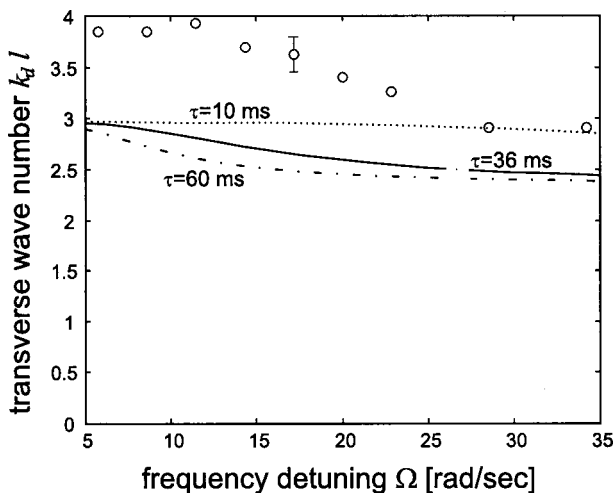


Fig. 10. Transverse wave number as a function of the frequency detuning $\Omega\tau$ for $\tau = 36$ ms (solid curve), $\tau = 10$ ms (dotted curve), and $\tau = 60$ ms (dashed-dotted curve) as predicted by the linear-stability analysis. Circles represent experimental values.

stant τ , where the deviation of the experimental values from the theoretical curves is minimal. The result of this analysis is depicted in Fig. 9 and shows the excellent agreement between theory and experiment for a parameter value of $\tau = 36$ ms. Here, circles depict the experimental results (normalized to the maximum value), and the solid curve represents the theoretical curve for the chosen parameter value τ . We also measured the buildup time of the photorefractive index grating to be $\tau_{\text{exp}} = 41$ ms. To see how sensitive the fit is to the variation of τ , Fig. 9 also contains the theoretical curves for the values $\tau = 31$ ms (dotted curve) and $\tau = 41$ ms (dashed curve). Even the latter one (which represents the value determined in experiment) shows a good approximation to the experimental results. For the optimum value of $\tau = 36$ ms the fit parameters were $\beta = 2.04$ and $\gamma = 5.31$.

Using the value of $\tau = 36$ ms, we can also compare the experimentally found values and the theoretical curve for

the unstable transverse wave number (normalized to the length of the crystal) $k_{q,l}$. In Fig. 10 these experimental values are shown as circles, whereas the solid curve is the theoretical one and is an excerpt from Fig. 4 for the parameter value $\tau = 36$ ms. Also here, curves for other parameter values are shown, for $\tau = 10$ ms (dotted curve) and $\tau = 60$ ms (dashed-dotted curve). One can clearly see that the slope of the curve was well reproduced by the straight line showing a slight decrease for larger frequency detunings Ω . Nevertheless, we see that the experimental values are larger by a factor of ~ 1.25 compared with the theoretical study. This deviation can be attributed to two facts, namely, measurement above threshold and absorption effects. Measurements were performed above threshold, which is known to cause larger transverse \mathbf{k} vectors² than predicted by the linear-stability analysis, which is only valid exactly at threshold. On the other hand, under real experimental conditions, a measurement slightly above threshold is always preferred for obtaining well-reproducible experimental results. Another fact that has to be taken into account is the presence of absorption in the material. As pointed out in Ref. 27, implementation of linear absorption into the analysis leads to an increase of the spatial frequency of the pattern. Figure 7(c) in Ref. 27 shows an increase of $\sim 5\%$ for an absorption of $al = 0.6$. Since the crystal we used was highly absorptive ($al \approx 1.2$), a contribution to the greater spatial frequency (approximately 10%–12%) of the experimental pattern can be attributed to absorption effects. Thus both contributions add and support the observed deviation.

As pointed out in Section 2, the linear-stability analysis predicts an instability even for unshifted frequencies of the two counterpropagating beams. This does not contradict previous analysis, where no instability was predicted. We assumed an additional frequency detuning δ in the sidebands with respect to the carrier in the analysis. For vanishing δ , threshold equation (28) can indeed be shown to have no solution for any parameter values $\Omega\tau$, in accordance with earlier results. The assumption of such a detuning is obviously necessary to observe spatial instabilities. In Fig. 5, one can clearly see that an instability for the case of external, counterpropagating beams is always connected with a nonzero value of the sideband frequency shift δ . Although we did not observe any transverse instability for $\Omega = 0$ in our experiment, the linear-stability analysis shows that a threshold coupling strength of $\gamma l = 5.25i$ is sufficient for modulational instability. The value of the coupling strength for the crystal we used in an experiment was lower than this value. This estimation is supported by the fact that we observed pattern formation only for a certain region in the frequency detuning Ω . A value of $\gamma l = 4.4i$, e.g., allows for observation of a δ_- instability in a certain range of the frequency detuning Ω , and at the same time this value is too low for observing an instability (δ_+ or δ_-) at $\Omega = 0$.

An important aspect of our experiment is the asymmetry in results concerning positive and negative detunings Ω . Pattern formation could only be achieved for positive values of Ω , which in the sign convention we use here means the amplified beam B is upshifted. This asymme-

try is also apparent in Fig. 3, where the minimum threshold for modulational instability is considerably lower for the case of positive frequency detunings. We have to note that including linear absorption into the analysis may raise the threshold curves.²⁷ However, our experiment fully supports the theoretically based prediction of a frequency window for transverse instability in the case of positive frequency detuning. Reversing the sign of Ω cancels the instability if the (larger) threshold coupling strength for negative detunings is not provided by the photorefractive nonlinearity.

Let us now discuss the physical relevance of a frequency detuning for pattern formation in this counterpropagating geometry. The externally supplied frequency shift Ω creates a real part of the coupling by substituting $\gamma \rightarrow \gamma/(1 + i\Omega\tau)$, and thereby photorefractive phase coupling comes into play. Therefore the threshold equation becomes complex, requiring an additional parameter, namely δ , to satisfy the threshold condition for both the real and the imaginary parts. We observed this δ -instability in our experiment and expect that a larger coupling constant would result in a transverse instability, even at $\Omega = 0$, but with nonzero δ . Thus we predict that, by use of a sample with a larger photorefractive coupling strength, $|\gamma l| \geq 5.25$, which was not within reach in the experiment we performed, a modulational instability can be found even for unshifted external beams.

In the research of Honda,¹⁴ where hexagons were first reported in an experiment with photorefractive nonlinearity, two different setups were used for obtaining transverse instability of two counterpropagating beams. The counterpropagating beam was created either by backreflection at the crystal backsurface (mirror boundary conditions) or by use of a photorefractive phase conjugator feeding back the laser beam into the crystal. In the second case an aperture was introduced in the feedback path in order to prevent the off-axis spatial sidebands from reaching the phase-conjugate mirror. Thus this situation is close to the conditions we consider in our research, the only difference being that a phase-conjugate signal was used in contrast to two external beams that are incident upon the crystal. Note that a BaTiO₃ phase conjugator is known to cause a small but nonzero frequency shift of ~ 1 Hz relative to the incoming beam.³³ Since we do not know the exact parameters of the Honda experiment (time constant τ of the KNbO₃ crystal, accuracy of alignment, and frequency shift of the counterpropagating phase-conjugate beam), we are limited to a qualitative discussion of these earlier results. Nevertheless, we note that nonstationary hexagons were reported in the presence of a frequency detuning that is similar to our observations with two slightly misaligned counterpropagating beams. The angle between the pump and the sidebands was reported to be $\sim 1^\circ$, which is comparable with our experimental results.

5. CONCLUSION

We have shown that counterpropagation in photorefractive two-wave mixing gives rise to modulational instabilities when the two beams are slightly detuned, even with-

out any external feedback. This is, to the best of our knowledge, the first experimental evidence of a transverse instability in a simple counterpropagating geometry with photorefractive nonlinearity and two external beams. The patterns that develop from the initial stage of modulational instability are found to be predominantly rolls. For slight induced misalignment, full hexagonal patterns develop. A linear stability analysis was presented to show the influence of the frequency detuning on the threshold coupling strength and the transverse wave number of the resulting pattern. The sidebands are typically detuned; i.e., running gratings in the transverse direction are created. The experiments underlined the asymmetry in Ω and supported the results of the linear-stability analysis. Measurements of the relative sideband intensity could be shown to be in good agreement with theoretical predictions; also theoretical values for the sideband angle were well reproduced in an experiment. An instability for unshifted beams ($\Omega = 0$) is predicted for crystal samples with a larger coupling constant.

ACKNOWLEDGMENTS

M. Schwab and C. Denz acknowledge kind support by T. Tschudi and helpful discussions with O. Sandfuchs. M. Schwab thanks the FAZIT-Stiftung and the Danish Research Academy for financial support. The experimental portion of this research was performed at Risø National Laboratory.

*Present address: Institut für Angewandte Physik, Westfälische-Wilhelms-Universität Münster, Corrensstrasse 2/4, D-48149 Münster, Germany.

†Present address: Department of Physics, 1150 University Avenue, University of Wisconsin, Madison, Wisconsin 53706.

REFERENCES AND NOTES

1. D. Walgraef, *Spatio-Temporal Pattern Formation* (Springer, New York, 1995).
2. M. C. Cross and P. C. Hohenberg, "Pattern formation outside of equilibrium," *Rev. Mod. Phys.* **65**, 851–1113 (1993).
3. M. A. Vorontsov and W. B. Miller, eds., *Self-Organization in Optical Systems and Applications in Information Technology* (Springer, Berlin, 1995).
4. G. Grynberg, E. Le Bihan, P. Verkerk, P. Simoneau, J. R. R. Leite, D. Bloch, S. Le Boiteaux, and M. Ducloy, "Observation of instabilities due to mirrorless four-wave mixing oscillation in sodium," *Opt. Commun.* **67**, 363–366 (1988).
5. J. Pender and L. Hesselink, "Degenerate conical emission in atomic sodium vapor," *J. Opt. Soc. Am. B* **7**, 1361–1373 (1990).
6. A. Petrossian, M. Pinar, A. Maître, J.-Y. Courtois, and G. Grynberg, "Transverse-pattern formation for counterpropagating beams in rubidium vapor," *Europhys. Lett.* **18**, 689–695 (1992).
7. S. N. Vlasov and E. V. Sheinina, "On the theory of interaction of counterpropagating waves in a nonlinear cubic medium," *Izv. Vyssh. Uchebn. Zaved. Radiofiz.* **26**, 20 (1983) [*Radiophys. Quantum Electron.* **27**, 15 (1983)].
8. W. J. Firth, A. Fitzgerald, and C. Pare, "Transverse instabilities due to counterpropagation in Kerr media," *J. Opt. Soc. Am. B* **7**, 1087–1097 (1990).
9. R. Macdonald and H. J. Eichler, "Spontaneous optical pattern formation in a nematic liquid crystal with feedback mirror," *Opt. Commun.* **89**, 289–295 (1992).

10. M. Tamburrini, M. Bonavita, S. Wabnitz, and E. Santamato, "Hexagonally patterned beam filamentation in a thin liquid-crystal film with a single feedback mirror," *Opt. Lett.* **18**, 855–857 (1993).
11. B. Thüring, R. Neubecker, and T. Tschudi, "Transverse pattern formation in liquid crystal light valve feedback system," *Opt. Commun.* **102**, 111–115 (1993).
12. R. Neubecker, B. Thüring, and T. Tschudi, "Formation and characterization of hexagonal patterns in a single feedback experiment," *Chaos, Solitons Fractals* **4**, 1307–1322 (1994).
13. J. Glückstad and M. Saffman, "Spontaneous pattern formation in a thin film of bacteriorhodopsin with mixed absorptive-dispersive nonlinearity," *Opt. Lett.* **20**, 551–551 (1995).
14. T. Honda, "Hexagonal pattern formation due to counterpropagation in KNbO₃," *Opt. Lett.* **18**, 598–600 (1993).
15. T. Honda, "Flow and controlled rotation of the spontaneous optical hexagon in KNbO₃," *Opt. Lett.* **20**, 851–853 (1995).
16. M. Saffman, D. Montgomery, A. A. Zozulya, K. Kuroda, and D. Z. Anderson, "Transverse instability of counterpropagating waves in photorefractive media," *Phys. Rev. A* **48**, 3209–3215 (1993).
17. A. V. Mamaev and M. Saffman, "Hexagonal optical patterns in anisotropic nonlinear media," *Europhys. Lett.* **34**, 669–674 (1996).
18. T. Honda, H. Matsumoto, M. Sedlatschek, C. Denz, and T. Tschudi, "Spontaneous formation of hexagons, squares and squeezed hexagons in a photorefractive phase conjugator with virtually internal feedback mirror," *Opt. Commun.* **133**, 293–299 (1997).
19. C. Denz, M. Schwab, M. Sedlatschek, T. Tschudi, and T. Honda, "Pattern dynamics and competition in a photorefractive feedback system," *J. Opt. Soc. Am. B* **15**, 2057–2064 (1998).
20. M. Schwab, C. Denz, and M. Saffman, "Multiple-pattern stability in a photorefractive feedback system," *Appl. Phys. B* **69**, 429–433 (1999).
21. M. Schwab, M. Sedlatschek, B. Thüring, C. Denz, and T. Tschudi, "Origin and control of dynamics of hexagonal patterns in a photorefractive feedback system," *Chaos, Solitons Fractals* **10**, 701–707 (1999).
22. P. M. Lushnikov and A. V. Mamaev, "Spontaneous hexagon formation in photorefractive crystal with a single pump wave," *Opt. Lett.* **24**, 1511–1513 (1999).
23. M. Saffman, A. A. Zozulya, and D. Z. Anderson, "Transverse instability of energy exchanging counterpropagating waves in photorefractive media," *J. Opt. Soc. Am. B* **14**, 1754–1760 (1994).
24. T. Honda and P. P. Banerjee, "Threshold for spontaneous pattern formation in reflection-grating-dominated photorefractive media with mirror feedback," *Opt. Lett.* **21**, 779–781 (1996).
25. A. I. Chernykh, B. I. Sturman, M. Aguilar, and F. Agulló-López, "Threshold for pattern formation in a medium with a local photorefractive response," *J. Opt. Soc. Am. B* **14**, 1754–1760 (1997).
26. O. Sandfuchs, J. Leonardy, F. Kaiser, and M. R. Belić, "Transverse instabilities in photorefractive counterpropagating two-wave mixing," *Opt. Lett.* **22**, 498–500 (1997).
27. O. Sandfuchs, F. Kaiser, and M. R. Belić, "Spatiotemporal pattern formation in counterpropagating two-wave mixing with an externally applied field," *J. Opt. Soc. Am. B* **15**, 2070–2078 (1998).
28. P. M. Lushnikov, "Hexagonal optical structures in photorefractive crystals with a feedback mirror," *Zh. Eksp. Teor. Fiz.* **113**, 1122–1135 (1998) [*JETP* **86**, 614–627 (1998)].
29. N. V. Kukhtarev, V. B. Markov, S. G. Odulov, M. S. Soskin, and V. L. Vinetskii, "Holographic storage in photorefractive crystals I+II," *Ferroelectrics* **22**, 949–964 (1979).
30. L. Solymar, D. J. Webb, and A. Grunnet-Jepsen, *The Physics and Applications of Photorefractive Materials* (Clarendon, Oxford, 1996).
31. In other experiments,⁴ it was shown that introduction of an angular misalignment breaks the symmetry and collapses a hexagonal pattern to a roll pattern. Here we see the opposite effect of a hexagonal pattern occurring only in the presence of a misalignment. Since the angular misalignment needed for a sufficient Bragg mismatch for hexagon formation ($\sim 0.1^\circ$) is much smaller than the angular scale of the pattern ($\sim 1^\circ$), the hexagonal symmetry is not broken.
32. C. Denz, J. Goltz, and T. Tschudi, "Enhanced four-wave mixing in photorefractive BaTiO₃ by use of tilted pump waves," *Opt. Commun.* **72**, 129–134 (1989).
33. K. R. MacDonald and J. Feinberg, "Enhanced four-wave mixing by use of frequency-shifted optical waves in photorefractive BaTiO₃," *Phys. Rev. Lett.* **55**, 821–824 (1985).
34. B. Ya. Zel'dovich, A. V. Mamaev, and V. V. Shkunov, *Speckle-Wave Interactions in Application to Holography and Nonlinear Optics* (CRC Press, Boca Raton, Fla., 1995), p. 256.